AIAA JOURNAL
Vol. 43, No. 8, August 2005

Characterization of Steady Blowing for Flow Control in a Hump Diffuser

Jonathan Luedke,* Paolo Graziosi,† Kevin Kirtley,‡ and Ciro Cerretelli§
General Electric Global Research, Niskayuna, New York 12309

A study has been performed to characterize the effects of steady boundary-layer injection on the separated flow of a hump diffuser. Results of parametrically varying discrete hole blowing characteristics have identified two separate regimes where the injection momentum coefficient and velocity ratio, respectively, are the primary scaling parameters for pressure recovery. Both discrete hole and slot injection have been investigated for varying degrees of adverse pressure gradient in the streamwise direction, indicating optimal discrete hole injection to be more efficient than slot injection in terms of necessary injection momentum coefficient to achieve maximum levels of increased pressure recovery. The effects of discrete injection parameters such as hole diameter, hole spacing, and streamwise injection (yaw) angle have been studied. Angled injection (45-deg yaw) has been shown to be most effective in removing separated flow and increasing the pressure recovery. The angled injection enhances shear layer mixing through large-scale corotating vortical motion induced by the yawed jet-main flow interaction. A computational fluid dynamics/data comparison study has been performed on the results of the discrete injection tests, capturing overall data trends and representing the net effect of streamwise and angled injection on pressure recovery in the hump diffuser.

Nomenclature

b	=	injection hole spacing
C_{p_o}	=	diffuser pressure recovery coefficient (data)
$C_{p_{o,a}}$	=	diffuser pressure recovery coefficient [computational fluid dynamics (CFD)]
C_{p_s}	=	local pressure recovery coefficient (data)
$C_{p_{s,a}}$	=	local pressure recovery coefficient (CFD)
C_μ	=	injected momentum coefficient
c	=	chord
d	=	injection hole diameter
h	=	height
l	=	injection hole length
m_b	=	injection mass flow
Re_c	=	chord-based Reynolds number
s	=	arc length
U_{fs}	=	freestream velocity
V_b	=	injection jet absolute velocity
V_R	=	injection velocity ratio
w	=	span
y^+	=	dimensionless wall distance
z	=	spanwise coordinate
α	=	upper diffusion wall angle
θ	=	injection hole streamwise angle
ρ	=	density
∞	=	ambient

Introduction

A STUDY has been performed to characterize the effects of steady boundary-layer injection into the separated flow of a hump diffuser. The motivation of the current study lies within the classic problem of boundary-layer separation in the presence of an adverse pressure gradient. This situation presents itself throughout the compression system of aircraft engines in highly loaded turbomachinery passages and transition ducts and is a limiter in engine performance and efficiency.[1] A great emphasis has recently been placed on assessing the merits of fluidic flow control in overcoming boundary-layer separation for such applications.[2–5] By the injection of small amounts of air taken from high-pressure engine sources into the near-wall region upstream of a separated flow, the boundary layer may be sufficiently energized to overcome the downstream adverse pressure gradient and avoid flow separation in aggressive engine components. Because the extraction of this high-pressure air results in a penalty on overall aircraft engine performance and efficiency, it is necessary to implement boundary-layer injection as efficiently as possible and minimize the flow requirements to achieve a net positive impact on engine performance. The intent of this study is to provide insights into the effectiveness of boundary-layer injection in preventing separated flow in an adverse pressure gradient and to characterize the impact of various geometric and flow injection parameters on diffuser pressure recovery to better design efficient fluidic injection schemes.

Both discrete and slot boundary-layer injection are investigated in this study. Direct comparisons are made to determine the more efficient method in terms of necessary flow requirements to achieve maximum pressure recovery in the hump diffuser. Diffuser pressure recovery is investigated as a function of both injected velocity and momentum to determine the most appropriate parameter in scaling the effects of injection scheme characteristics on pressure recovery levels. The results of the discrete injection test are compared with corresponding computational fluid dynamics (CFD) predictions to assess the capabilities of current design tools in capturing the effects of boundary-layer injection on a separated flow.

Experimental Design

The General Electric (GE) Global Research Center (GRC) diffuser rig model, aft looking forward, is shown in Fig. 1. The lower wall contour of the test model under investigation (Fig. 2) is designed to produce a streamwise pressure distribution representative of that found on the suction surface of a highly loaded compressor stator blade. This distribution provides an unanchored, naturally separated flow pattern downstream of the crest and includes the streamline curvature seen in compressor blades. Seifert et al.[6] and

Received 13 August 2004; presented as Paper 2004-4963 at the 22nd Applied Aerodynamics Conference, Providence, RI, 16–19 August 2004; accepted for publication 17 February 2005.

*Mechanical Engineer, Engineering Systems 220A, Energy and Propulsion Technologies. Member AIAA.
†Aeronautical Engineer, Engineering Systems 204, Energy and Propulsion Technologies.
‡Aeronautical Engineer, Engineering Systems 205, Energy and Propulsion Technologies.
§Aeronautical Engineer, Engineering Systems 510, Energy and Propulsion Technologies. Member AIAA.

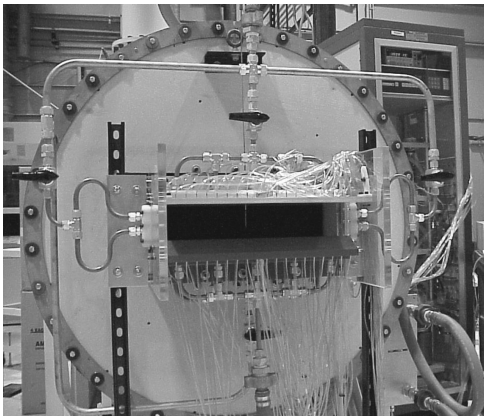

Fig. 1 GE GRC diffuser test rig, aft looking forward.

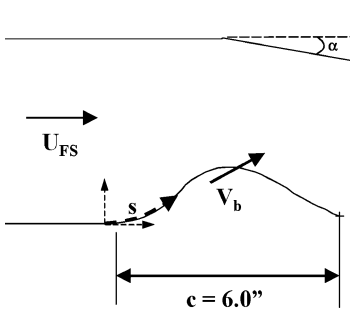

Fig. 2 Hump diffuser cross section.

Viken et al.[7] have studied a similar hump model; however, the separated flow over the hump was anchored by a highly convex surface. The rig is an open-circuit flow system, exhausting into ambient. The upper and sidewalls of the model are flat and result in a cross section at the crest of the lower hump with aspect ratio of 6. Fences are placed 0.25 chord lengths from the sidewalls to minimize the effects of sidewall boundary layers and, therefore, reduce flow three dimensionalities along the span. Flow control is introduced along the span of the model at the location of the crest of the hump, just upstream of the line of natural separation. The streamwise pressure gradient is adjusted by changing the configuration of the model upper wall, which is hinged above the crest of the lower surface (Fig. 2). This allows for comparison of the effectiveness of injection configurations in the presence of a progressively stronger adverse pressure gradient downstream of the crest. Results corresponding to two pressure distributions are reported on here: a stronger adverse gradient produced with a level upper wall ($\alpha = 0$ deg) and a weaker adverse gradient with the wall inclined down ($\alpha = -5$ deg).

The model has been designed to allow for easy implementation of various flow control configurations. The surface area along the crest of the hump where flow control in the form of steady blowing is applied consists of a removable insert that completes the contour of the hump. When this portion of the lower surface is made removable, injection patterns may be changed without requiring any alterations to the overall rig. A plenum, which is fed by five equally distributed 1-in. (25.4-mm)-diam pipes, is fixed to the bottom of the flow control insert to provide a uniform flow source.

A direct current blower is used to supply the main flow to the diffuser. Secondary air for flow control is supplied by 90-psi (620.5-kPa) house air. The main flow is delivered to a settling chamber through a shallow angle diffuser, designed with an expansion angle of 7 deg to avoid boundary-layer separation. The 48-in. (1.22-m)-diam settling chamber is fitted with a layer of aluminum honeycomb to suppress any swirl and lateral mean velocity variations exiting the diffuser. Immediately downstream of the honeycomb are two rows of 0.125-in. (3.18-mm)-thick perforated plates to suppress longitudinal mean velocity variations and reduce the inlet turbulence intensity.[8] Downstream of the plates, an elliptical bell mouth transitions to the 4.8×20 in. (122×508 mm) rectangular cross section. Because of the large aspect ratio of the duct cross section, an optimized bellmouth design is not practical. An inlet wire mesh is located at the exit of the bellmouth to reduce any spanwise nonuniformities resulting from the design.

Baseline, no flow control test conditions correspond to a freestream velocity of 85 ft/s (2.16 m/s) and Re_c of 3×10^5. The freestream condition is defined at center span, center height, and 0.3 chord lengths upstream of the hump model leading edge (origin of coordinate system in Fig. 2). Trip wires made of 0.010-in. (0.25-mm)-diam wire are placed along the perimeter of the duct upstream of the test section to ensure turbulent transition for the incoming low-Reynolds-number flow.

Diffuser Measurements

Measurements and Performance Metrics

The diffuser test rig is instrumented with 164 static pressure taps along the upper and lower flowpath walls. A schematic of the locations of the pressure taps is provided in Fig. 3, with $s/c = 0$ defined at the hump leading edge (Fig. 2). Four rows of spanwise taps with 1-in. (25.4-mm) spacing are located along the lower wall at 0.12, 0.64, 0.81, and 0.90 chord lengths downstream of the hump leading edge. Two rows of spanwise taps are located along the upper wall at 0.12 and 0.90 chord lengths (measured with upper wall at $\alpha = 0$ deg). An axial row of taps equally spaced at an arc length of 0.25 in. (6.35 mm) is located along the centerline of both the upper and lower walls. The freestream flow condition, as identified in the experimental design section, is monitored through a pitot–static pressure probe and a subsonic venturi located in the upstream supply piping. The mass flow rate and pressure of the secondary flow control air are also monitored during the tests.

Two key performance metrics are considered, the local pressure recovery coefficient C_{p_s} and the overall diffuser pressure recovery coefficient C_{p_o}, as defined in Eqs. (1) and (2). C_{p_s} is calculated along the centerline of the lower wall to monitor the pressure recovery distribution along the hump contour, whereas C_{p_o} provides a measure of the overall diffuser performance. The crest dynamic head is approximated in these quantities by the difference between the freestream total pressure measured upstream of the test section and the spanwise averaged crest static pressure. Because C_{p_s} and

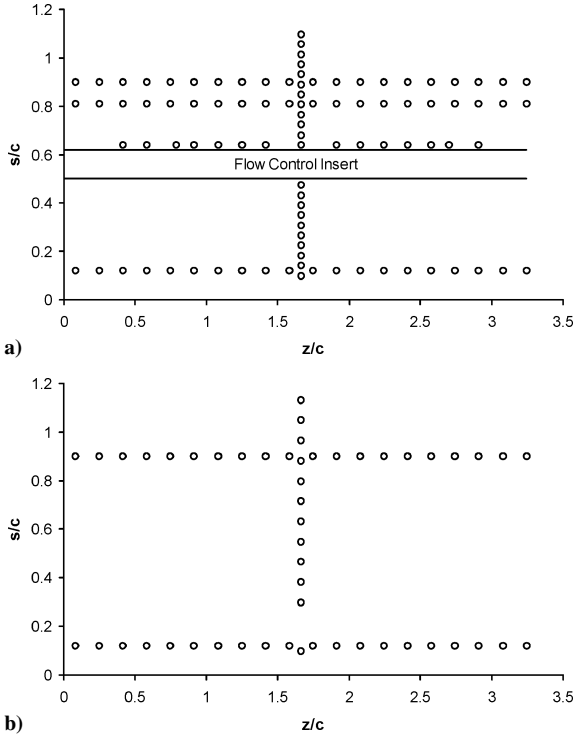

Fig. 3 Layout of wall static pressure taps on model walls: a) lower and b) upper.

C_{p_o} are relative performance measures and are consistently defined throughout the study, this approximation is deemed adequate. Thus,

$$C_{p_s} = \frac{P_s(s) - \bar{P}_{s,\text{crest}}}{P_{t,\text{fs}} - \bar{P}_{s,\text{crest}}} \tag{1}$$

$$C_{p_o} = \frac{P_{s,\text{amb}} - \bar{P}_{s,\text{crest}}}{P_{t,\text{fs}} - \bar{P}_{s,\text{crest}}} \tag{2}$$

Data Acquisition

A Scanivalve system with six 48-port modules, each with a dedicated differential pressure transducer, is used to monitor the pressure signals from the 164-wall static pressure taps as well as the freestream pitot–static probe. Scanivalve data are sampled through a National Instruments E-Series 16-bit high-frequency data acquisition board at a rate of 20 Hz for a period of 10 samples after a 2-s settling time. The frequency content cutoff of measured pressure signals in the separated flow region has been experimentally shown to be less than 5 Hz, indicating that sampling rates greater than 10 Hz are free from aliasing. This low-frequency content is likely due to the damping provided by the length of small diameter plastic tubing connecting each pressure tap to the measurement port and is not related to the actual frequency content of the flow unsteadiness. The effect of the number of samples on the measurements has been studied, and 10 samples have been shown to be adequate to determine the actual mean pressure values. The 2-s settling time has been shown through testing to be adequate for allowing the pressure port volume to equilibrate. Additional differential pressure transducers monitoring venturi and settling chamber temperatures and pressures are channeled through a Validyne CD280 carrier demodulator and sampled through a National Instruments FP1600 field point system. Statistics from the field point measurements are recorded and phased with the mean and standard deviation of pressures measured for each Scanivalve port. When the statistics time interval for the field point data is set to some time less than the total time of one complete Scanivalve rotation (48 ports), each set of statistical field point data is guaranteed to be representative of the same flow condition of the corresponding Scanivalve rotation data. A schematic detailing the configuration of the data acquisition system is shown in Fig. 4.

Measurement Error

An analysis of measurement capabilities has been performed on the measurement system of the current study to assess the repeatability and reproducibility of pressure measurements. For this assessment, each flow control insert is assembled in the diffuser rig, tested, removed, and then reassembled and retested to determine the random error due to the measurement system and the part-to-part variability. This assessment has been performed for the $\alpha = -5$ deg diffuser configuration in terms of overall pressure recovery levels C_{p_o} for the baseline, no flow control condition. A one-way analysis of variance of the test data gives a measurement standard deviation due to repeatability error of $\pm 0.01 C_p$, with a ratio of part-to-part variability to measurement variability of ~27. These results indicate

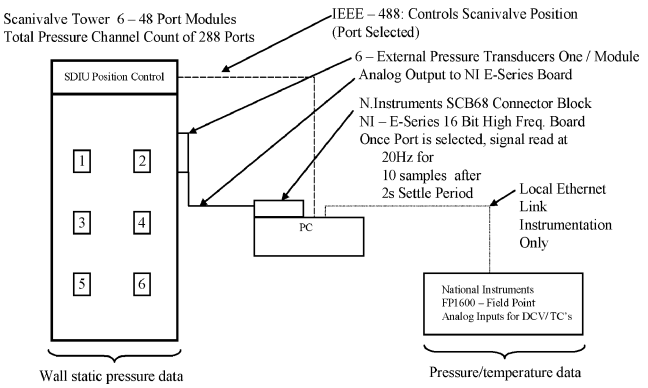

Fig. 4 Schematic of data acquisition system.

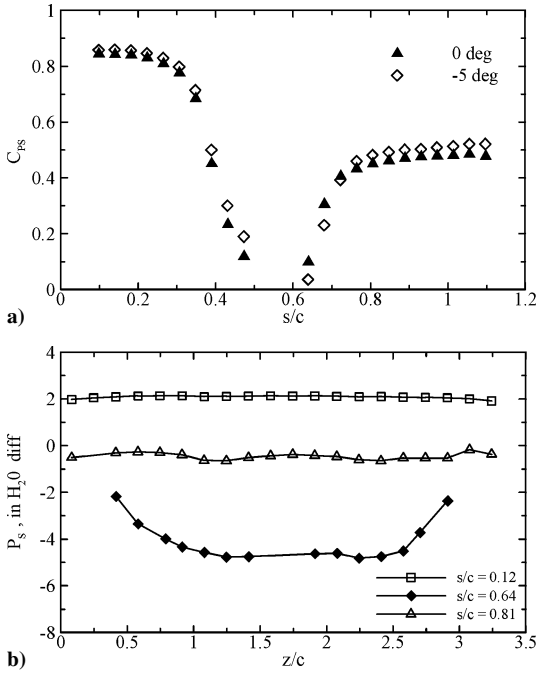

Fig. 5 Baseline, no flow control diffuser performance: a) baseline local pressure recovery curves along lower surface for $\alpha = 0$ and -5 deg and b) spanwise lower wall pressure distribution at $s/c = 0.12$, 0.64, and 0.81 ($\alpha = -5$ deg).

that measured differences in C_{p_o} due to different characteristics are well above the level of expected measurement noise.

Geometric tolerances are specified as ±0.003 in. (0.08 mm).

Baseline, No-Flow Control Tests

Baseline, no-flow control tests have been performed to assess the reference pressure distribution through the model in the presence of separated flow. These tests are run at a mass flow rate of 4.2 lbm/s (1.91 kg/s), corresponding to a freestream velocity of 85 ft/s (2.16 m/s). The midspan, streamwise lower surface pressure distribution is plotted in terms of C_{p_s} in Fig. 5a for both the $\alpha = 0$ deg and $\alpha = -5$ deg diffuser configurations. Because the $\alpha = 0$ deg configuration has a larger expansion area distribution, the associated pressure recovery increases at a slightly steeper rate than the $\alpha = -5$ deg configuration just downstream of the crest ($0.64 < s/c < 0.75$). However, this larger expansion area also creates a stronger adverse pressure gradient in the diffuser, and therefore, the separation point moves upstream relative to the $\alpha = -5$ deg configuration, resulting in a lower exit pressure recovery level. Shown in Fig. 5b are the spanwise pressure distributions for the lower wall pressure tap rows located in the accelerating region of the hump, $s/c = 0.12$; at the crest, $s/c = 0.64$; and in the diffusion region, $s/c = 0.81$. The lower surface inlet flow appears quite uniform across the span, whereas the distribution at the crest shows significant sidewall pressure deficits. This sidewall deficit is likely because the weak corner flow along the base of the fences separates earlier than the midspan flow. This nonuniformity is seen to have dissipated by $s/c = 0.81$, where a near constant pressure distribution is found across the span within the separated region.

Discrete Injection Characterization

Discrete Injection Parameters

A series of discrete injection flow control configurations have been tested to determine the effect that each of a series of flow and geometric parameters has on the lower wall pressure recovery distribution. The parameters considered in the study are injection hole diameter d, injection hole spacing b, injection hole yaw orientation θ, injection momentum coefficient C_μ, and velocity ratio V_R, with parameter ranges indicated in Table 1. Each combination of flow control parameters is tested under both the $\alpha = 0$ and -5 deg

Table 1 Range of parameters considered in discrete injection study

Injection parameter	Minimum value	Maximum value
b, in. (mm)	0.3 (7.6)	0.9 (22.9)
d, in. (mm)	0.032 (0.81)	0.052 (1.32)
θ, deg	0	45
C_μ	0	6%
V_R	0	7.7
l/d	6.5	
Pitch, deg	20	

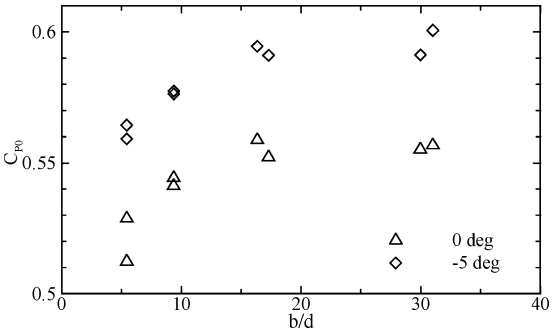

Fig. 6 Baseline diffuser performance as a function of injection configuration *b/d*.

upper wall configurations to determine their relative effectiveness in a progressively stronger adverse pressure gradient.

A total of eight injection configurations are investigated in the format of a three-parameter, full factorial design of experiment (DOE). A separate flow control insert is constructed for each test, with the full design space represented by each combination of the extreme values of b, d, and θ. The injection pitch angle relative to the hump surface and the ratio l/d for the holes are kept constant.

The pressure recovery coefficient is interrogated as a function of both injected momentum coefficient and velocity ratio to determine an appropriate scaling parameter. These parameters are defined as

$$C_\mu = \frac{m_b V_b}{\left(\frac{1}{2}\rho U_{\text{fs}}^2 c w\right)_{\text{baseline}}} \tag{3}$$

$$V_R = \frac{V_b}{(U_{\text{fs}})_{\text{baseline}}} \tag{4}$$

Each flow control insert is tested across a range of plenum pressures leading to the ranges of injection momentum and velocity ratio defined in Table 1.

Note that the representative injection jet velocity V_b is calculated based on the measured injection total temperature and mass flow rate and the crest wall static pressure approximately 0.25-in. (6.35-mm) arc length downstream of injection.

Effect of Injection Hole Configuration on Baseline Diffuser Performance

Baseline testing in the diffuser rig uncovers a dependency of the no flow control overall pressure recovery levels on the flow control insert geometry. As shown in Fig. 6, as the ratio of b/d increases, the baseline overall pressure recovery level increases nearly logarithmically, varying by approximately 0.05 across the range investigated. Increasing the ratio of b/d implies either an increase in the injection hole spacing b, and thus a reduction in the total number of holes, or a decrease in injection hole diameter d. The resulting different levels of local surface disturbance introduced by each flow control insert are suggested as the reason for the observed difference in diffuser pressure recovery. Because of the design of the DOE, four levels of b/d are investigated with two configurations per level of b/d. From Fig. 6, it is seen that the overall pressure recovery at each replicated level of b/d collapses fairly well.

Pressure Recovery with Discrete Injection

By the varying of the flow control plenum pressure, a series of injection momentum and velocity ratios are realized for each test. The resulting overall model pressure recovery levels for each flow control insert configuration are interrogated as a function of both quantities to determine the most appropriate parameter as a design-scaling factor. Diffuser pressure recovery coefficients plotted as functions of injection momentum coefficients and velocity ratios are shown in Figs. 7–10 for diffuser configurations of $\alpha = 0$ and -5 deg. Note that the curves are labeled in the order of injection hole diameter, hole spacing, and yaw orientation angle. The trend of increasing baseline, no flow control pressure recovery with increasing b/d

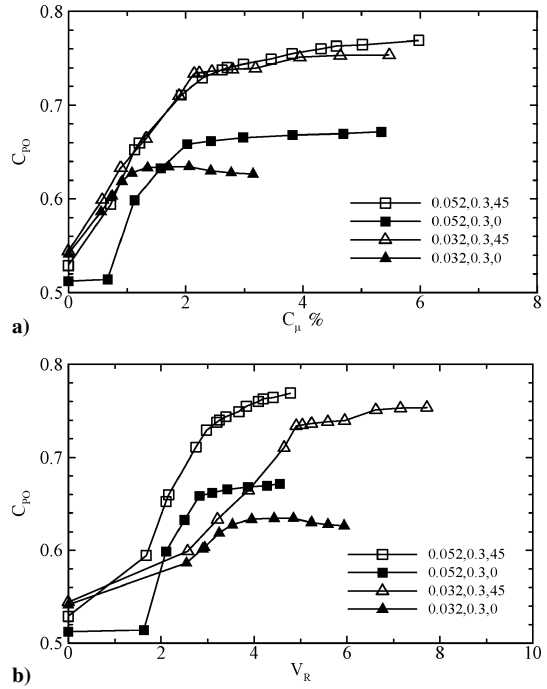

Fig. 7 Discrete injection diffuser pressure recovery curves for *b* = 0.3 in. (7.62 mm) as a function of a) C_μ and b) V_R for $\alpha = 0$ deg.

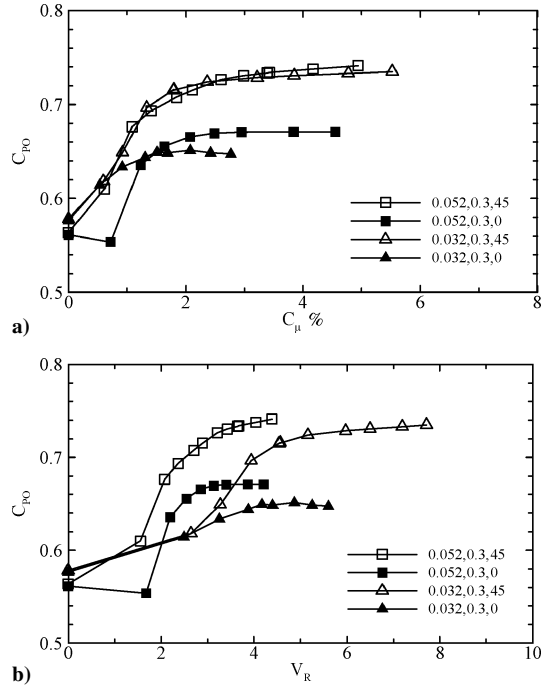

Fig. 8 Discrete injection diffuser pressure recovery curves for *b* = 0.3 in. (7.62 mm) as a function of a) C_μ and b) V_R for $\alpha = -5$ deg.

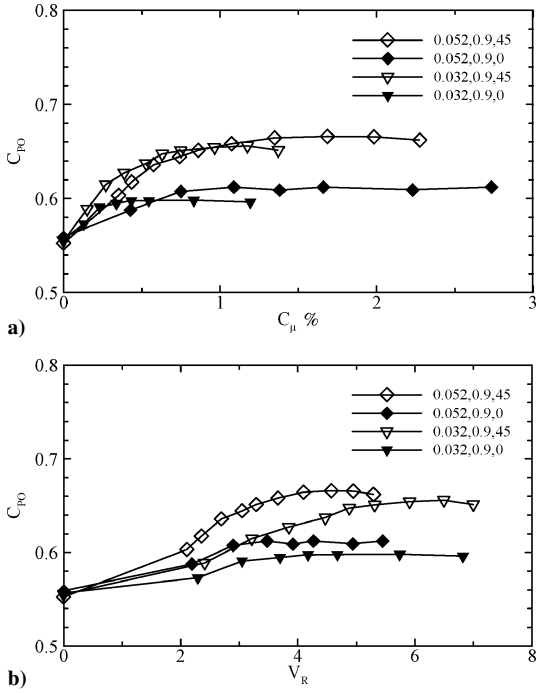

Fig. 9 Discrete injection diffuser pressure recovery curves for b = 0.9 in. (22.9 mm) as a function of a) C_μ and b) V_R for $\alpha = 0$ deg.

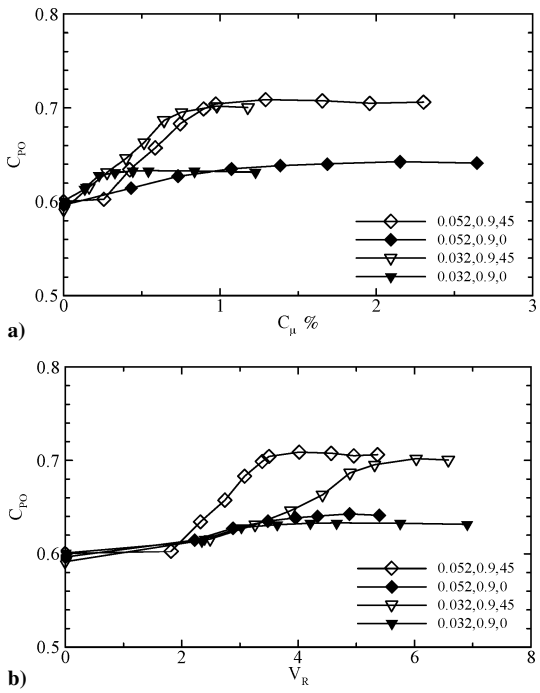

Fig. 10 Discrete injection diffuser pressure recovery curves for b = 0.9 in. (22.9 mm) as a function of a) C_μ and b) V_R for $\alpha = -5$ deg.

demonstrated in Fig. 6 is again demonstrated in each of Figs. 7–10 at C_μ and $V_R = 0$.

Within the design space of this set of experiments, no apparent scaling of diffuser pressure recovery with velocity ratio is evident (Figs. 7b, 8b, 9b, and 10b). However, the effect of hole diameter on the pressure recovery coefficient appears to scale with the momentum coefficient, particularly for the case of yaw angle equal to 45 deg (Figs. 7a, 8a, 9a, and 10a). This finding of momentum scaling is consistent with that reported by Kwong and Dowling for the case of wall injection in a conical diffuser.[9] In general, yawed ($\theta = 45$ deg) injection is found to be far more effective than straight injection, producing significantly higher pressure recovery levels. The greater effectiveness with yawed injection is arguably due to the more effective momentum transfer produced by the dominant vortex resulting from the interaction of a pitched and skewed (yawed) jet over that of the weak trailing vortex pair produced by a pitched streamwise jet, as suggested by Johnston and Khan.[10]

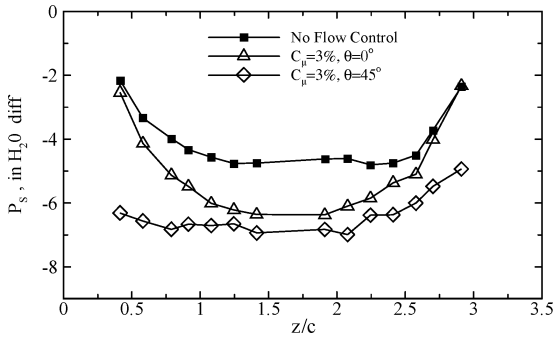

Fig. 11 Crest spanwise lower wall pressure distributions with and without flow control ($\alpha = -5$ deg), d = 0.052 in. (1.32 mm), and b = 0.3 in. (7.62 mm).

Injection hole spacing is found to have a small effect on maximum pressure recovery level in the presence of the weaker pressure gradient with $\alpha = -5$ deg (Figs. 8 and 10), although for momentum coefficients less than approximately 1%, the larger hole spacing is more efficient, requiring nearly 50% less momentum to achieve similar levels of pressure recovery. This is suggested to be due to a reduced level of boundary-layer disturbance created by a reduced number of injection jets for the larger hole spacing configuration at a relatively low injection momentum. For the stronger pressure gradient ($\alpha = 0$ deg), the maximum pressure recovery levels achieved using the larger hole spacing are approximately 7–12% less than those achieved with the smaller hole spacing.

The less consistent momentum scaling and reduced pressure recovery levels achieved with streamwise injection ($\theta = 0$ deg) are likely to be related to the fact that the boundary layer does not uniformly recover across the entire span of the diffuser with these configurations. Shown in Fig. 11 are the spanwise lower wall pressure distributions downstream of injection at the crest of the hump ($s/c = 0.64$) for three test cases: baseline, no flow control; 0.052-in. (1.32-mm) diameter, 0.3-in. (7.62-mm) spacing, streamwise injection with 3% momentum; and 0.052-in. (1.32-mm) diameter, 0.3-in. (7.62-mm) spacing, 45-deg yaw injection with 3% momentum. The baseline condition again shows a fairly nonuniform pressure distribution across the span. A spanwise pressure gradient is also apparent for the flow control cases. In the case of 45-deg yaw injection, the pressure distribution remains relatively flat near $z/c = 0$, whereas the opposite end of the distribution shows a region of higher static pressure leading to the sidewall at $z/c = 3.0$. Because the angled injection jets are oriented toward the sidewall near $z/c = 3.0$, this high-pressure region is believed to be due to stagnation build up along the sidewall fence. The pressure values with injection are significantly lower across the diffuser span compared to baseline because the flow is further accelerated at the crest due to reduced blockage and a reattached boundary-layer flow. In the case of streamwise injection, a strong nonuniformity exists across the span, indicating that the boundary layer may not be fully reattached with flow control along the span. Whereas pressure levels at the center of the diffuser span approach those achieved with 45-deg yaw injection, the weaker sidewall flow corresponds to reduced overall pressure recovery levels achieved with streamwise injection.

As a result of the eight-parameter experimental study, injection spacing of 0.3 in. (7.62 mm) and 45-deg yaw orientation is found to give the greatest increase in diffuser overall pressure recovery. Equal levels of recovery are achieved for both the 0.052-in. (1.32-mm) and 0.032-in. (7.62-mm)-diam injection hole configurations due to the collapse of pressure recovery curves with injection momentum ratio (Figs. 7 and 8). In Fig. 12, the midspan streamwise pressure recovery distribution along the lower surface for baseline, no flow control and 0.052-in. (1.32-mm) diam, 0.3-in. (7.62-mm) spacing, 45-deg yaw injection with 3% momentum are compared. Whereas

Table 2 Geometric features of slot and hole insert

Parameter	Value
Discrete hole insert	
d, in. (mm)	0.075 (1.91)
b, in. (mm)	0.3 (7.62)
θ, deg	0, 45
l/d	5, 6.5
A_{open}, in.^{2} (mm^2)	0.24 (154)
Slot insert	
h, in. (mm)	0.016 (0.41)
w, in. (mm)	16.2 (411)
l/h	6.5
A_{open}, in.^{2} (mm^2)	0.26 (168)

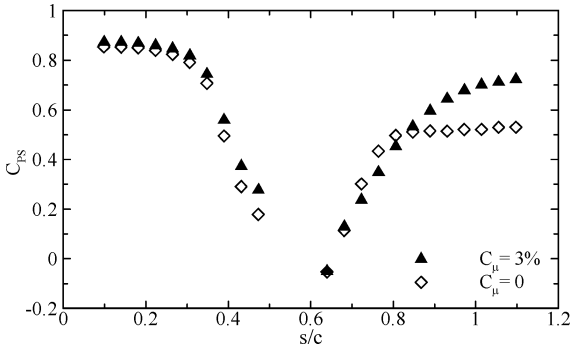

Fig. 12 Centerline local pressure recovery distribution along lower wall for baseline and 0.052-in. (1.32-mm) diameter, 0.3-in. (7.62-mm) spacing, and 45-deg injection.

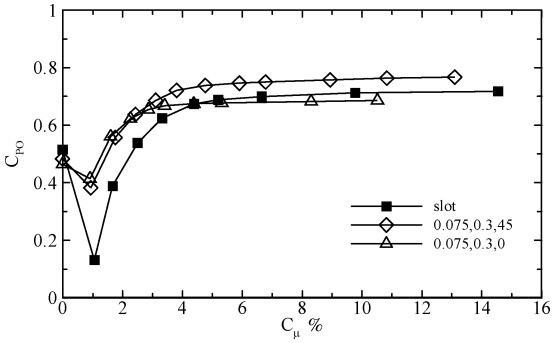

Fig. 13 Diffuser pressure recovery curves for slot and discrete injection as a function of injected momentum ($\alpha = 0$ deg).

the baseline pressure recovery levels off due to flow separation near $s/c = 0.75$, the pressure recovery with flow control continuously increases throughout the diffusion region. The improved overall pressure recovery due to flow control is represented here by the significant increase in C_{p_s} at the exit of the model ($s/c \sim 1.1$).

Slot Injection Characterization

Boundary-layer separation control by means of slot injection has been investigated to compare the effectiveness of this technique relative to discrete hole injection. To do so, a set of approximately equal open area injection configurations has been tested. The geometric characteristics of these configurations are summarized in Table 2. The slot is compared to discrete injection configurations with the optimal hole spacing of 0.3 in. (7.62 mm) identified in the discrete injection characterization section, and at yaw injection angles of 0 and 45 deg. Each injection scheme is tested under both the $\alpha = 0$ and -5 deg upper wall configurations to determine their relative effectiveness in a progressively stronger adverse pressure gradient.

The pressure recovery coefficients resulting from slot injection and the equivalent open area discrete injection are plotted in Fig. 13

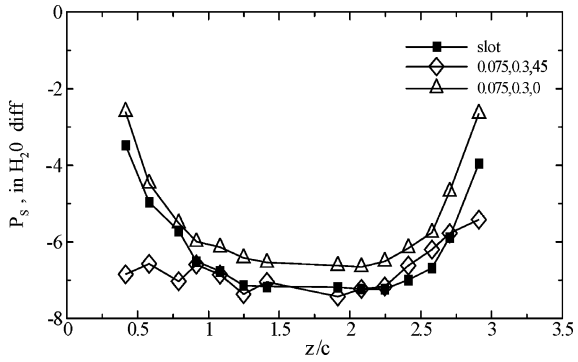

Fig. 14 Crest spanwise lower wall pressure distributions for slot and corresponding discrete injection ($\alpha = 0$ deg).

as functions of injected momentum for the diffuser configuration of $\alpha = 0$ deg. Yawed injection ($\theta = 45$ deg) produces greater pressure recovery than streamwise injection, consistent with what was discussed in the preceding section. Observe that the baseline pressure recovery with the slot is slightly higher than that of the corresponding discrete injection. It is suggested that this initial higher diffuser performance is due to reduced surface drag introduced by the smoother, continuous slot configuration. The no-blowing slot pressure recovery value falls in line with the trend established in Fig. 6 of baseline diffuser performance scaling with the open area associated with the injection configuration. However, as soon as injection is initiated, the pressure recovery coefficient falls to low values lower than 0.2. This drop in performance is likely because, at very low velocity ratios, injection perturbs the flow stream and may promote earlier separation. The slot introduces this disturbance over the entire span rather than at a finite number of locations as in the case of discrete injection. This is such that, at low C_μ, slot injection has a worse effect on the diffuser performance than its discrete counterpart, whether the holes are streamwise (0 deg) or yawed (45 deg).

For the milder diffuser pressure gradient distribution ($\alpha = -5$ deg), the slot achieves approximately the same level of pressure recovery as the 45-deg holes for high values of injection momentum, although it requires almost twice the amount of injection momentum (not shown). When the pressure gradient is stronger ($\alpha = 0$ deg), however, the recovery levels due to slot injection are lower across the entire range of momentum coefficient (Fig. 13).

The less effective performance of the slot is arguably due to the absence of the enhanced mixing induced by the strong streamwise vorticity generated by 45-deg yawed injection. When the crest pressure distribution in Fig. 14 is examined, it is seen that in the near-corner lower wall regions, where the boundary layer is weaker, the streamwise hole and the slot injection do not yield fully reattached flow.

Scaling Laws for Discrete Injection

As discussed in the section on discrete injection characterization, a series of discrete injection insert configurations have been tested to characterize the effect of a number of flow and geometric parameters on the diffuser pressure recovery. Within the design space of these experiments, the effect of hole diameter on the pressure recovery coefficient appears to scale with momentum coefficient for the yawed injection case (Figs. 7–10). No apparent scaling is present when the pressure recovery coefficient is plotted against the velocity ratio at either diffuser angle.

One might argue, however, that the momentum coefficient cannot be the scaling parameter for all injection hole diameters. In fact, as the size of the holes is increased indefinitely and the momentum level held constant, a condition will be reached where the injection jet velocity becomes so low as to lose its effectiveness. This appears evident by looking at the results of the experiments discussed in the section on slot injection characterization, where both the slot and the equivalent open area discrete insert show a marked decrease in performance when $C_\mu < 2\%$ and correspondingly $V_R < 1$ (Fig. 13).

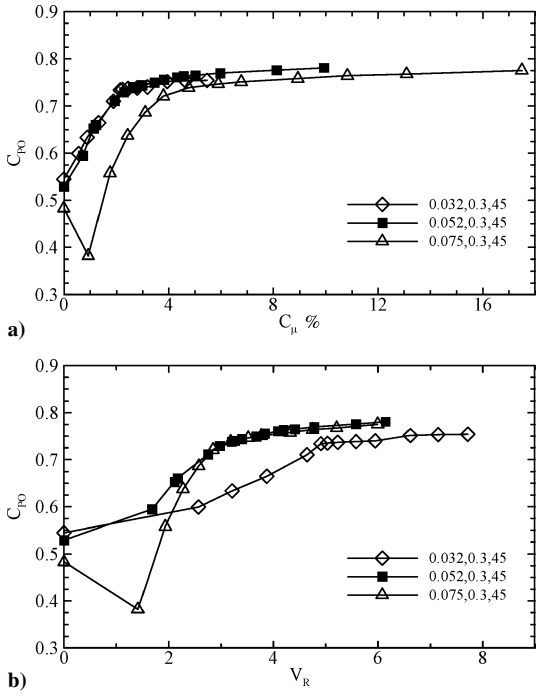

Fig. 15 Discrete injection scaling of hole diameter with moment and velocity ratios: a) diffuser pressure recovery curves as a function of C_μ for $\alpha = 0$ deg and b) diffuser pressure recovery curves as a function of V_R for $\alpha = 0$ deg.

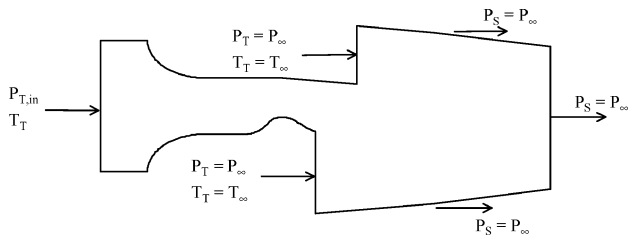

Fig. 16 Geometry schematic used in CFD predictions of wall injection in hump diffuser.

To better understand these scaling laws, a series of injection hole diameters in the range 0.032 in. (0.81 mm) $< d <$ 0.075 in. (1.91 mm) have been compared for yawed ($\theta = 45$ deg) injection. In Fig. 15, the pressure recovery coefficients are plotted vs momentum coefficient (Fig. 15a) and velocity ratio (Fig. 15b). It is apparent that there are two separate regimes where the injection momentum coefficient and the velocity ratio, respectively, scale the effect of hole diameter on pressure recovery coefficient. The momentum coefficient appears to be the proper scaling parameter for $d \leq 0.052$ in. (1.32 mm), whereas the velocity ratio appears to be the proper scaling parameter for $d \geq 0.052$ in. (1.32 mm).

CFD Data Match of Discrete Injection Tests

Introduction

A CFD study has been performed to compare to the experimental results of the discrete hole injection tests. A commercially available code (CFX 5.6) was used for the simulations. The effects of parameters such as turbulence model and mesh resolution are investigated to assess the capabilities of CFD in representing measured trends in diffuser pressure recovery due to injection. Both baseline and injection with 0.052-in. (1.32-mm)-diam holes and 0.3-in. (7.62-mm) hole spacing, streamwise and yawed are investigated with a diffuser upper wall configuration of $\alpha = -5$ deg. A three-dimensional grid spanning one injection hole with translational periodicity on each side is used. A schematic of the geometry cross section used in the predictions is shown in Fig. 16 with all boundary conditions identified. The model begins upstream of the bellmouth with a uniform total pressure and total temperature inlet boundary condition. At the discharge of the diffuser model a plenum is attached to represent the ambient room that flow exhausts into. This plenum has been found to be a necessary element of the geometry to represent accurately the diffuser discharge conditions. The upstream surfaces of the plenum are treated as inlet boundaries with ambient conditions imposed as uniform total pressure and total temperature. These surfaces are treated as inlets to resolve entrainment created by the exhaust jet shear layers at the edges of the discharge section. The remaining surfaces of the plenum are treated as outlet boundaries with uniform ambient static pressure imposed. Preliminary calculations have ruled out any effect of the size of the discharge plenum on the predicted development of the exhaust jet.

For simulations of boundary-layer injection, both streamwise and yawed, the actual injection hole length is modeled. The length of the hole is consistent with the l/d realized in the experiment. Uniform total pressure and total temperature corresponding to those measured in the injection plenum are imposed at the inlet face of the injection hole.

Alternative pressure recovery coefficients $C_{p_{s,a}}$ and $C_{p_{d,a}}$, defined in Eqs. (5) and (6), are used for CFD comparisons of local and overall diffuser pressure recovery, respectively. These definitions are based on the inlet freestream total and static pressures and are preferred over the initial crest pressure based definitions [C_{p_s} and C_{p_o} in Eqs. (1) and (2)] due to pressure spikes along the crest in the CFD predictions resulting from a spurious severe pressure gradient at the point of injection. Thus,

$$C_{p_{s,a}} = \frac{P_s(s) - P_{s,\mathrm{fs}}}{P_{t,\mathrm{fs}} - P_{s,\mathrm{fs}}} \tag{5}$$

$$C_{p_{o,a}} = \frac{P_{s,amb} - P_{s,\mathrm{fs}}}{P_{t,\mathrm{fs}} - P_{s,\mathrm{fs}}} \tag{6}$$

CFD Predictions of Baseline, No-Blowing Test Data

The baseline, no-blowing test condition has been simulated with a range of turbulence models and levels of grid resolution. To assess the accuracy of each prediction, the resulting centerline lower surface $C_{p_{s,a}}$ distribution is compared to that from the test data. First the level of grid resolution is assessed. Three grids are considered, each defined by the average dimensionless wall distance value y^+ along the lower hump surface. These grids are characterized by average y^+ values of 19, 7, and 5. Note that in CFX 5.6 an automatic near-wall treatment is applied that automatically switches from wall functions to a low Reynolds number near-wall formulation as the mesh is refined.[11] The spanwise resolution is consistently set at a uniform 2.5 cells/d [where $d = 0.052$ in. (1.32 mm)] for each grid. Predictions based on the k–ω turbulence model are shown here, with similar trends found for the k–ε and Shear Stress Transport (SST) models. Shown in Fig. 17 are the lower wall midspan streamwise $C_{p_{s,a}}$ distributions for each grid. The coarsest grid, with an average y^+ of 19, is found to overestimate the diffusion through the diffuser and predict separation farther downstream than is inferred by the data. However, the results corresponding to the next two levels of refinement (average y^+ of 7 and 5) show very good agreement with the data. Because no significant change in pressure distribution is

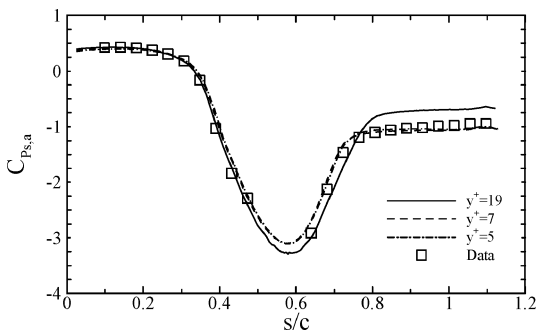

Fig. 17 CFD predictions of baseline lower wall centerline $C_{p_{s,a}}$ distribution for three levels of grid resolution, k–ω turbulence model.

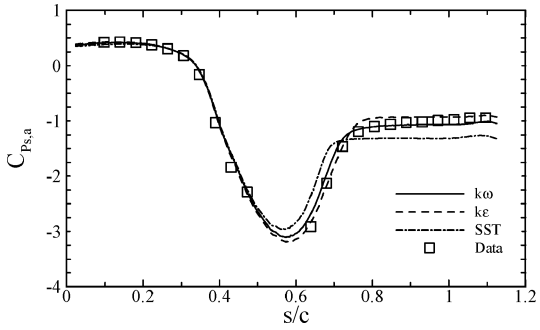

Fig. 18 CFD predictions of baseline lower wall centerline $C_{p_{s,a}}$ distribution with k–ω, k–ε, and SST turbulence models at average lower wall y^+ of 5.

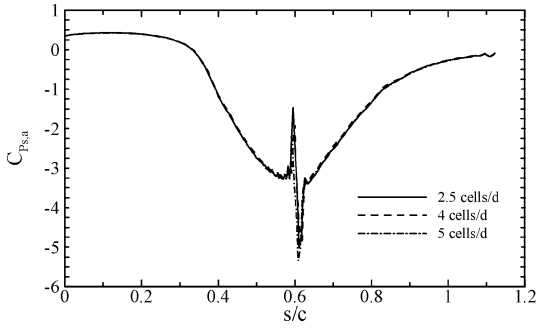

Fig. 19 CFD predictions of lower wall $C_{p_{s,a}}$ distribution with 3% momentum streamwise injection for three levels of spanwise mesh resolution.

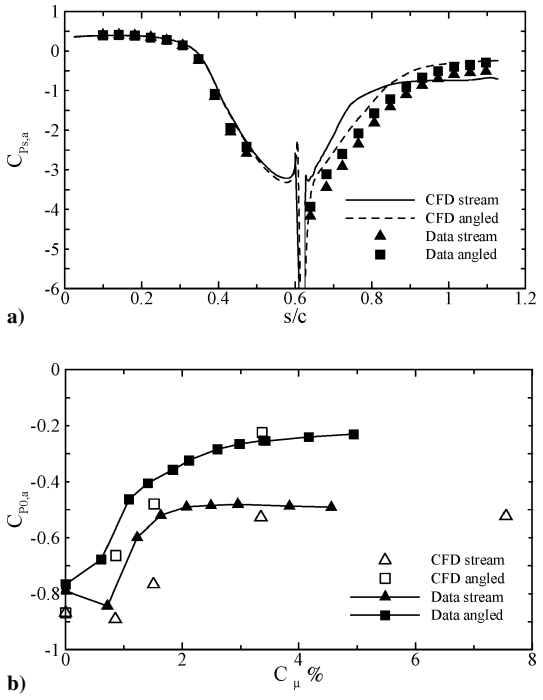

Fig. 20 CFD predictions: a) lower wall $C_{p_{s,a}}$ distribution with 3.4% momentum for streamwise and yawed injection and b) overall diffuser pressure recovery $C_{p_{o,a}}$ as a function of injection momentum coefficient for streamwise and yawed injection.

found between these grids, an average y^+ of 5 along the lower wall is deemed appropriate for a grid-independent result.

Whereas the k–ω turbulence model is seen in Fig. 17 to match the baseline pressure recovery distribution very well with an average y^+ of 5 along the lower wall, two additional turbulence models are also considered, SST and k–ε. Results of predictions with each turbulence model at an average lower wall y^+ of 5 are shown in Fig. 18. The SST model, generally well suited for predicting the onset of boundary-layer separation in an adverse pressure gradient, in this case incorrectly predicts the location of the point of separation when compared with data. The predicted pressure recovery at the exit of the duct is underpredicted by approximately 25% with the SST model. Both the k–ω and k–ε models well predict the pressure recovery through the diffuser; however, the k–ω model more accurately captures the point where the diffuser pressure recovery levels off as a result of separation. As a result of these findings, the predictions of boundary-layer injection are run with the k–ω turbulence model at a grid resolution of average y^+ of 5 along the lower surface.

CFD Predictions of Boundary-Layer Injection

The discrete injection test case of 0.052-in. (1.32-mm)-diam holes with 0.3-in. (7.62-mm) spacing is simulated for both streamwise and 45-deg yawed injection. Predictions of both the distribution of local pressure recovery and the overall diffuser pressure recovery are compared with data to assess the capabilities of CFD in representing the net performance improvement measured with yawed injection over that with streamwise injection.

An additional assessment of mesh refinement is performed to determine the effect of span-wise resolution across a single injection hole spacing. Again, three levels of refinement are considered, with uniform cell spacing of 2.5, 4, and 5 cells per injection hole diameter at the point of injection. The average lower wall y^+ value for each mesh is 5. The results of streamwise injection with 3% momentum for each mesh are shown in Fig. 19. The pressure spikes at the point of injection alluded to earlier are apparent in Fig. 19. Although the magnitude of this spike varies between meshes, the actual distribution of pressure recovery along the hump does not depend on the mesh size. The coarser mesh (2.5 cells/d) is used for the predictions to limit the overall mesh size.

CFD predictions of both streamwise and yawed injection are carried out over a range of injected momentum coefficients. The results of the predictions are found to capture the overall data trends. As seen in Fig. 20a, although predictions with flow control do not exactly match the measured centerline pressure recovery distribution in the case of streamwise injection, they do capture well the general trends in pressure recovery realized with yawed injection. Note that, for an equivalent level of injected momentum, the predicted exit pressure recovery ($s/c = 1.1$) is higher for the case of yawed injection than for the case of streamwise injection. Additionally, the overall diffuser pressure recovery with injected momentum coefficient shown in Fig. 20b shows that CFD qualitatively reproduces the data trends. A higher injected momentum is, however, required in predictions to obtain maximum levels of pressure recovery. The discrepancies are arguably a result of the modeling inconsistency where a spanwise nonuniformity is measured in experimental data, whereas a periodic boundary condition is imposed at the sides of a single injection hole with the CFD model.

Contour plots from CFD predictions along the lower diffuser surface show significantly higher levels of streamwise vorticity with yawed injection when compared to those corresponding to the streamwise injection case. This is demonstrated in Fig. 21, where contours of streamwise vorticity along the lower surface from point of injection to hump trailing edge are plotted for both the streamwise and yawed injection cases, each for a 3.4% injection momentum coefficient. Yawed injection is seen to produce regions of high positive streamwise vorticity values, arguably associated with corotating primary vortices that persist along the entire length of the hump wall, whereas streamwise injection results in the generation of secondary counter-rotating vortices that dissipate by midchord. The vortex patterns due to streamwise injection appear to be similar to those reported by Fric and Roshko.[12] This finding supports the claim that enhanced pressure recovery due to yawed injection is likely provided by improved mixing through large-scale corotating vortical motion induced by the yawed jet-main flow interaction.

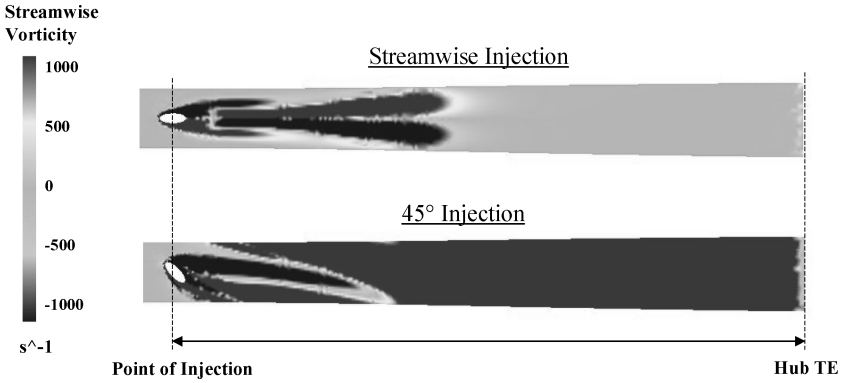

Fig. 21 CFD contours of streamwise vorticity along lower surface due to streamwise and yawed injection at a momentum coefficient of 3.4%.

Conclusions

Steady blowing flow control has been investigated in a hump diffuser as a means of preventing boundary-layer separation due to an adverse pressure gradient. Discrete hole injection has been analyzed to determine the optimum injection configuration in terms of hole diameter, hole spacing, and hole orientation (yaw angle). Yawed injection ($\theta = 45$ deg) has been shown to be the most effective configuration, with significantly higher pressure recovery arguably due to enhanced shear layer mixing induced by large scale corotating vortices resulting from the jet–main flow interaction. Test results have identified two separate ranges of injection hole diameter where the effect of hole diameter on diffuser pressure recovery coefficient scales with the injected momentum coefficient and velocity ratio, respectively. For the design space considered, results with smaller injection hole diameters scale with injected momentum coefficient, whereas results with larger injection hole diameters scale with injected velocity ratio. Both hole and slot injection have been tested, with discrete injection capable of achieving increased pressure recovery at reduced levels of momentum injection.

The results of the discrete injection tests have been compared with corresponding CFD predictions to assess the capabilities of current design tools in capturing the effects of boundary-layer injection on a separated flow. With use of CFX 5.6, the baseline no flow control condition is well predicted using the k–ω turbulence model with an average lower wall y^+ of 5. Both streamwise and yawed injection have been considered, with overall data trends captured in predictions representing the general trends of streamwise and angled injection on pressure recovery in the hump diffuser.

References

[1]Lord, W. K., MacMartin, D. G., and Tillman, T. G., "Flow Control Opportunities in Gas Turbine Engines," AIAA Paper 2000-2234, 2000.

[2]Jenkins, L., Althoff Gorton, S., and Anders, S., "Flow Control Device Evaluation for an Internal Flow with an Adverse Pressure Gradient," AIAA Paper 2002-0266, 2002.

[3]Lin, J. C., Howard, F. G., Bushnell, D. M., and Selby, G. V., "Investigation of Several Passive and Active Methods for Turbulent Flow Separation Control," AIAA Paper 90-1598, 1990.

[4]Walker, S., "Lessons Learned in the Development of a National Cooperative Program," AIAA Paper 97-3348, 1997.

[5]Washburn, A. E., Althoff Gorton, S., and Anders, S., "Snapshot of Active Flow Control Research at NASA Langley," AIAA Paper 2002-3155, 2002.

[6]Seifert, A., and Pack, L. G., "Active Control of Separated Flows on Generic Configurations at High Reynolds Numbers," AIAA Paper 99-3403, June 1999.

[7]Viken, S. A., Vatsa, V. N., Rumsey, C. L., and Carpenter, M. H., "Flow Control Analysis on the Hump Model with RANS Tools," AIAA Paper 2003-218, 2003.

[8]Mehta, R. D., and Bradshaw, P., "Design Rules for Small Low Speed Wind Tunnels," *Aeronautical Journal of the Royal Aeronautical Society*, Vol. 73, Nov. 1979, pp. 443–449.

[9]Kwong, A. H., and Dowling, A. P., "Active Boundary-Layer Control in Diffusers," *AIAA Journal*, Vol. 32, No. 12, 1994, pp. 2409–2414.

[10]Johnston, J. P., and Khan, Z., "The Origins of the Dominant Vortex from a Pitched and Skewed Jet," *Proceedings of the International Conference on Fluids Engineering*, Vol. 1, Japan Society of Mechanical Engineering, 1997, pp. 321–326.

[11]CFX 5.6, Software Documentation, 2003, p. 86.

[12]Fric, T. F., and Roshko, A., "Vortical Structures in the Wake of a Transverse Jet," *Journal of Fluid Mechanics*, Vol. 279, 1994, pp. 1–47.

H. Reed
Associate Editor